A PARAMETRIC STUDY OF THE SOLAR WIND INTERACTION WITH COMETS

C. T. Russell, G. Le, J. G. Luhmann

Institute of Geophysics and Planetary Physics, University of California, Los Angeles, California 90024-1567

J. A. Fedder

Naval Research Laboratory, Washington, D. C. 20375

Abstract. The Naval Research Laboratory's magnetohydrodynamic simulation code is used to simulate the solar wind interaction with comet Halley for two different outgassing rates and several different solar wind states. The magnetic field is more strongly draped for fast solar wind conditions than slow. For higher mass loading rates, the tail becomes wider and contains more magnetic flux. The visual appearance of the comet differs for the case in which the interplanetary magnetic field lies in the plane of the sky from the case when it lies along the line of sight. The ion tail appears shorter in the latter case. Thus variation in the IMF direction can cause significant changes in the appearance of comets. The comet also creates a large momentum flux deficit in the solar wind with a narrow enhanced region within it corresponding to the ion tail.

Introduction

To date in-situ measurements are available from only two comets. Much has been learned from these encounters but nevertheless the sampling has been limited in terms of spatial coverage and the variety of solar wind conditions and cometary outgassing rates studied. Despite the paucity of in-situ data, it is important to investigate the behavior of cometary tails as best we can. First, cometary ion tails are well-studied optically from the Earth, and second, the Earth itself may have once passed through a cometary tail while relevant terrestrial data were being recorded [cf. Russell et al., 1988].

Comets encounter a variety of solar wind conditions during an apparition, both because of their varying heliocentric distance and because of the temporal variations in the solar wind. Furthermore, as they pass through the inner solar system their outgassing rate increases and then decreases. There are many cometary phenomena that appear to be controlled by the solar wind or interplanetary magnetic field [cf. Niedner and Brandt, 1978; Jockers, 1985]. The only well understood response is the change in tail direction due to a solar wind directional change. The causes of most other phenomena are merely conjectures.

An important advance in our ability to understand comets was the development of magnetohydrodynamic (MHD) simulations [Schmidt and Wegmann, 1980;1982]. These codes do not simulate all of the physical (or chemical) processes occurring in the comet but they do reproduce at least semi-quantitatively the deceleration of the solar wind and the pile up of the magnetic field. Furthermore, they produce a simulated comet that can be probed throughout a volume of space rather than solely along a spacecraft trajectory. It is the purpose of this paper to examine one such MHD simulation, that performed by Fedder et al. [1986], as a function of varying cometary and solar wind parameters to elicit which parameters control what features of a comet. The simulation results used will be in steady state or quasi-steady state conditions. Nevertheless, it is anticipated that by examining these steady state conditions there will be clues as to the causes of dynamic phenomena in comets as transitions between these steady states. It is also hoped that these simulations will aid cometary researchers in determining what parameters should be examined when studying the observed response of comets to changes in the solar wind.

The MHD simulation used here was developed at the Naval Research Laboratory and has been described by Fedder et al. [1986]. The comet is taken to be a spherically symmetric outgassing body releasing gas of atomic weight 20 amu which expands at 1 km/sec. The ionization rate is taken to be 10^{-6} sec^{-1} and due solely to photoionization. The equations of continuity, momentum and pressure, and Faraday's, Ampere's and Ohm's law are then solved on a mesh of dimension 33 x 29 x 29 extending 2.4 million km upstream and 7.6 million km downstream

Cometary Plasma Processes
Geophysical Monograph 61
©1991 American Geophysical Union

Table 1. Parameters Used in Simulations

Name of run	VEGA	Slow	Normal	Fast
Production Rate (1.0E30/molecules/sec	1.3	0.6	0.6	0.6
Solar Wind Velocity (km/sec)	450	330	450	700
Solar Wind Density (amu/cc)	9	12	9	4
Solar Wind Momentum Flux (nPa)	3.04	2.18	3.04	3.27
IMF (nT)	7	7	7	7
Te (ev)	10	10	10	10
Tp (ev)	10	3	10	20

and 1.2 million km to the north, south, east and west of the nucleus. The numerical algorithm used is a partial donor cell method. The code uses free slip boundary conditions on the top and bottom and sides in which the tangential component of velocity has zero derivative at the boundary. The back surface has a slight drop (10%) in pressure across it. The interplanetary magnetic field is perpendicular to the solar wind flow in this model.

The observed magnetic field profile has been compared with the comet simulation by Schwingenschuh et al. [1986; 1987]. The observed magnetic field profile differs significantly from the predicted profile only close to the nucleus where the distance to the nucleus approaches the mesh spacing of the simulation. The simulation also predicts convection time delays similar to those observed [Schwingenschuh et al., 1987].

We examine herein the results of four simulation runs. The first run is for the conditions most typical of the solar wind at the location of the VEGA and GIOTTO encounters, which we term normal solar wind, [cf. Feldman et al., 1977] and for a mass loading rate close to that observed during the GIOTTO encounter 0.6×10^{30} molecules per second (1.2×10^{31} amu s^{-1}), [Reinhard, 1986]. The second simulation is for conditions typical of a slow solar wind; the third for a fast solar wind. The fourth simulation keeps the conditions for a typical solar wind but increases the outgassing rate to a value close to that observed during the VEGA encounters, 1.3×10^{30} molecules per second (2.6×10^{31} amu s^{-1}), [Gringauz et al., 1986]. The parameters used in these runs are given in Table 1. We note that the solar wind momentum flux does not vary much between these runs even though the other parameters do. This behavior is an observed property of the solar wind. The standard deviation of the momentum flux in the solar wind is only about 8% of its mean value [Feldman et al., 1977].

The plan of the paper is as follows. To introduce the simulation and its parametric dependences we will examine the draped magnetic field pattern for the various runs. Then we examine the integrated line of sight density to determine how the comet might look to an observer under these varying conditions. A preliminary report on these results has been presented elsewhere [Russell et al., 1989] but these results are repeated here so that the results in the later sections of the paper may be properly understood. Next we examine the variation of the magnetic field direction, density, velocity and momentum flux for different models and distances down the tail using contour plots on cross-sections of the tail.

Magnetic Field Line Draping

Figure 1 shows the magnetic field lines in the plane containing the solar wind flow, the upstream magnetic field and the cometary nucleus for the slow, normal and fast solar wind runs at the GIOTTO mass loading rate and for normal solar wind conditions at the VEGA rate. The choice of lines to be drawn was governed by a desire to provide a representation of the field strength while not saturating the plot with field lines in the regions of maximum field. Since the magnetic field strength is proportional to the number of magnetic field lines crossing a unit area perpendicular to the field and since this area is determined by two dimensions (one parallel to the solar wind flow and one into the page) we spaced field lines along the x-axis through the comet inversely proportional to the square root of the field strength and traced the field lines upward and downward from the x-axis. Hence field lines are not equispaced in time in this display. All four runs show the strongly draped field configuration expected for a comet of the size of Halley. As a measure of the amount of draping we take the intersection of the field line

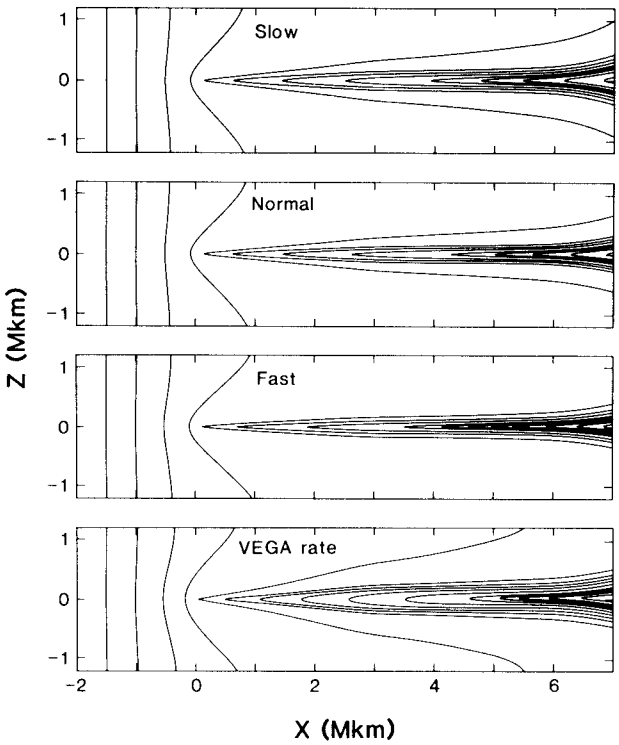

Fig. 1. From top to bottom, magnetic field lines in the plane containing the nucleus for slow solar wind, normal solar wind and fast solar wind for a mass loading rate of 0.6 x 10^{30} molecules per second. The bottom panel shows the magnetic field lines for normal solar wind conditions and a mass loading rate of 1.3 x 10^{30} molecules per second. [Russell et al., 1989].

passing through the nucleus with the sides of the simulation box. The closer is this field line to the x-axis, the more strongly draped is the tail. The draping is stronger for the faster flowing solar wind which produces a more tightly confined tail. The increased mass loading rate field line configuration is most like that of the slow solar wind, strongly draped but with a somewhat wider tail than those of the normal and fast solar wind runs.

Figure 1 also reveals some of the limitations of this MHD model. We would expect for instance that the tail plasma would accelerate with distance from the nucleus. This would cause field lines to spread apart in x. This occurs in Figure 1 to distances of 4 to 5x10^6 km. However after this point the field lines begin to approach each other representing an increasing field with distance from the nucleus. Similarly we see an increasing flare beyond about 6x10^6 km. These artifacts are most probably respectively due to the inability of the finite cell-size to treat the narrow current layer in the distant tail and the growing influence of the rear simulation boundary over the sides as the flow approaches the end of the simulation space. While the reader should be aware of these imperfections, we feel the accuracy of the simulation is sufficient to provide the lessons concerning cometary behavior for which this paper is intended.

Line-of-Sight Integrated Densities

In order to determine how the comet should appear visually, we must first separate the solar wind ions from the cometary ions and then integrate the number of cometary ions along the line-of-sight. To separate the solar wind ions we note that the solar wind mass flux is divergenceless, i.e.,

$$\nabla \cdot \rho_{sw} \underline{V}_{sw} = 0 \qquad (1)$$

This can be determined from the MHD solution by taking the numerical divergence appropriate for the Partial Donor Cell method used in the computations:

$$\Sigma_\alpha \nabla_\alpha (S_\alpha V_\alpha M_\alpha^+ (\rho)) = 0 \quad (\alpha = X,Y,Z) \qquad (2)$$

$$\text{where } \nabla f_j = f_j - f_{j-1}$$

$$M^+ f_j = 1/2 (f_j + f_{j+1})$$

where S is the area of the face of a cube in the computational grid and α denotes the direction of each component or operator in the Cartesian grid. This equation is used to determine the downstream value of the mass flux from the previous upstream value, thus allowing the determination of the mass flux added by the comet (which is not divergenceless).

The favorable comparison between the calculated magnetic field profile and that observed by the VEGA spacecraft [Schwingenschuh et al., 1986; 1987] gives us confidence in the model's applicability. The observed magnetic field profile differs significantly from the predicted profile only close to the nucleus where the distance to the nucleus approaches the grid spacing of the simulation. The simulation also predicts convection times similar to those observed.

The integrated density of cometary ions shown in Figures 2-5 has been calculated along the line-of-sight for two orientations of the interplanetary magnetic field with the observer at infinity perpendicular to the solar wind flow. In the top panel of each display the magnetic field is perpendicular to the line-of-sight, and in the bottom panel along it. Thus in the top panel the observer is looking along the thickest part of the ion tail and in the lower panel across the thinnest part of the sheet. Figure 2 shows contour plots for the normal solar wind case. As one would expect the tail visually extends further from the comet when the magnetic field is perpendicular to the line-of-sight than when it is along it. Thus simple rotations of the IMF about the solar wind flow vector can cause the cometary ion tail to appear to lengthen or shorten without any real change in the comet.

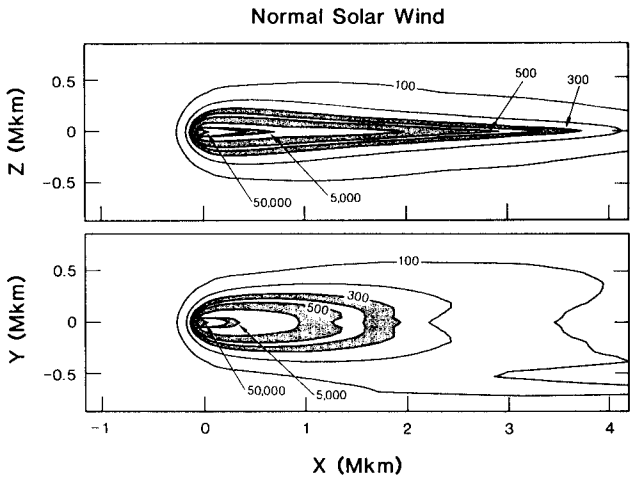

Fig. 2. Line-of-sight integrations of the cometary ion density for the normal solar wind run with a mass-loading rate of 0.6 x 10^{30} molecules s^{-1}. Top panel shows the projection into the plane containing the interplanetary magnetic field. Bottom panel shows the projection into the orthogonal plane. Integrated densities are given in units of 10^{10} ions cm^{-2}. [Russell et al., 1989].

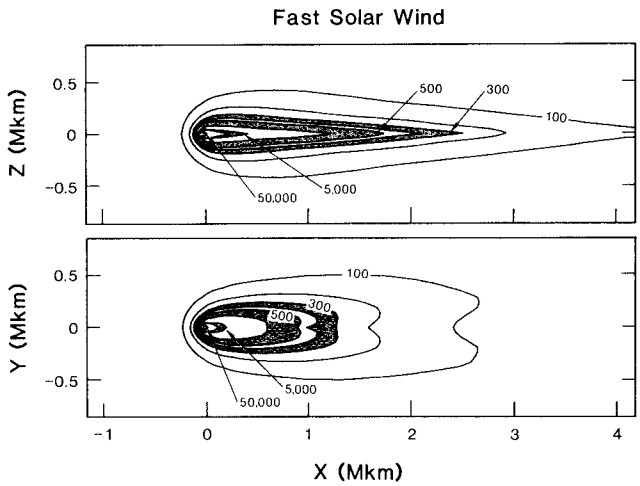

Fig. 3. Line-of-sight integrated cometary ion densities similar to Figure 3 but for fast solar wind. [Russell et al., 1989].

Figure 3 shows the analogous displays for the fast solar wind. Here the difference between the two orthogonal views is less because the ion sheet is not so ribbon-like. The ion tail, perhaps counter-intuitively is shorter. This occurs because the fast solar wind carries cometary ions away faster so that the density does not build up to as high a value. Figure 4 shows the integrated cometary ion density for the slow solar wind. As expected from the comparison of the normal and fast solar wind cases, the slow solar wind causes a much longer visible tail because the ion density builds

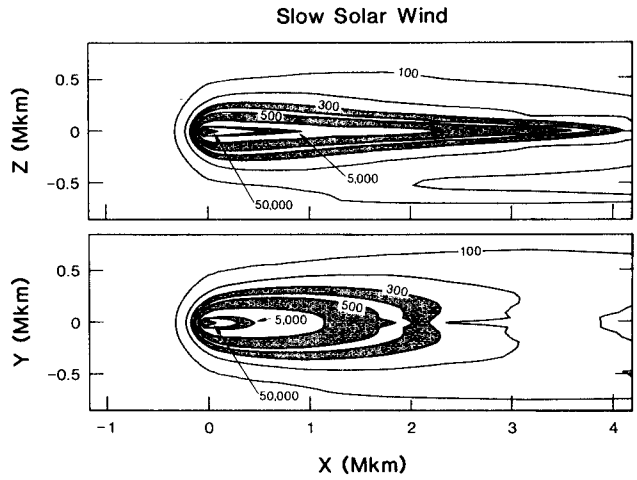

Fig. 4. Line-of-sight integrated cometary ion densities similar to Figure 3 but for slow solar wind. [Russell et al., 1989].

up to higher values when the flow is slower. Since the ion sheet here is thin and ribbon-like the difference in the orthogonal views is quite marked. Figure 5 shows the integrated cometary ion density

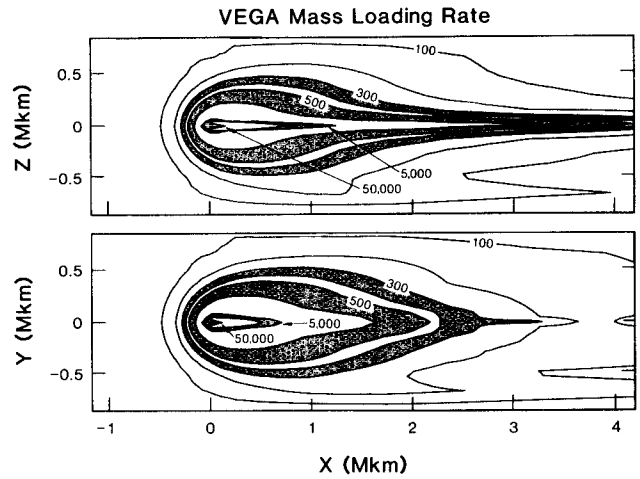

Fig. 5. Line-of-sight integrated cometary ion densities similar to Figure 3 but for outgassing rates similar to those encountered by VEGA. [Russell et al., 1989].

for the higher mass loading rate appropriate to the VEGA encounters. The difference in the two views is again quite marked, even more so than at lower mass loading rates. As in all of these cases, the tail is longer when viewed orthogonal to the magnetic field and shorter when viewed along it. Closer to the nucleus we find that the cometary ion density is greater at all orientations of the field for this higher mass loading rate and extends further upstream.

The cometary magnetic tail and its ion tail are not coincident. The greatest ion density lies at

the sharp kink in the magnetic field and extends in a ribbon whose thinnest dimension is in the vertical direction in Figure 1 and whose width is in the direction into the page. Thus, the integrated density along the line-of-sight will vary depending on whether the observer is sighting along the thickest or thinnest dimension of the ion tail

Cross-sections of the Cometary Wake

One of the dominant visual features of a comet is its plasma tail. Surrounding this plasma, or ion tail, is an unseen magnetic tail with enhanced magnetic field and reduced momentum flux. In order to characterize this region which must play an important role in the dynamics of cometary tails we have examined the value of various parameters across the cross-section of the tail at two distances downstream from the nucleus, 1 x 10^6 km and 6 x 10^6 km. Figure 6 shows contour maps of the mass density for these two distances for the three models: normal solar wind, the VEGA mass loading rate and the fast solar wind cases. We do not present contour maps of the slow solar wind case because they are very similar to those of the VEGA mass loading case as can be inferred from a comparison of Figures 4 and 5. No symmetry has been assumed in these simulations so that the observed symmetry and deviations from it are some indication of the level of numerical artifacts and transient effects. In each panel the upstream magnetic field is horizontal.

The middle panel shows the mass densities for the normal solar wind. At 1 x 10^6 km there is a moderately narrow ribbon of high densities near the center of the tail elongated in a direction perpendicular to the magnetic field. The maximum density here is 1000 amu cm^{-3}. Further from the tail axis are two lunes of low densities beyond which the density rises. At 6 million km the ribbon of high density has become pinched into 2 narrower ribbons but the density has fallen by 2 orders of magnitude to 11 amu cm^{-3}. The density minima to the sides are still present but their shape has evolved from lunes to tear drops. The minimum density at 6 x 10^6 km is about 1/4 that at 1 x 10^6 km.

The top two panels show the fast solar wind model. Here the density is less than in the normal solar wind case by a factor of about 2 to 3 at both 1 and 6 x 10^6 km distances. Generally the contours have the same shape as in the normal solar wind case. The high mass loading rate model shown in the bottom two panels shows a similar pattern. The densities in the ion tail are a factor of about 3 greater here than in the normal solar wind case with slightly over a factor of 2 smaller mass loading rate. There are no lobes of minimum density to the sides of the ion tail at 1 x 10^6 km but such lobes have developed, albeit weakly, at 6 x 10^6 km.

Figure 7 shows the corresponding contours for the magnetic field strength. Examining the normal

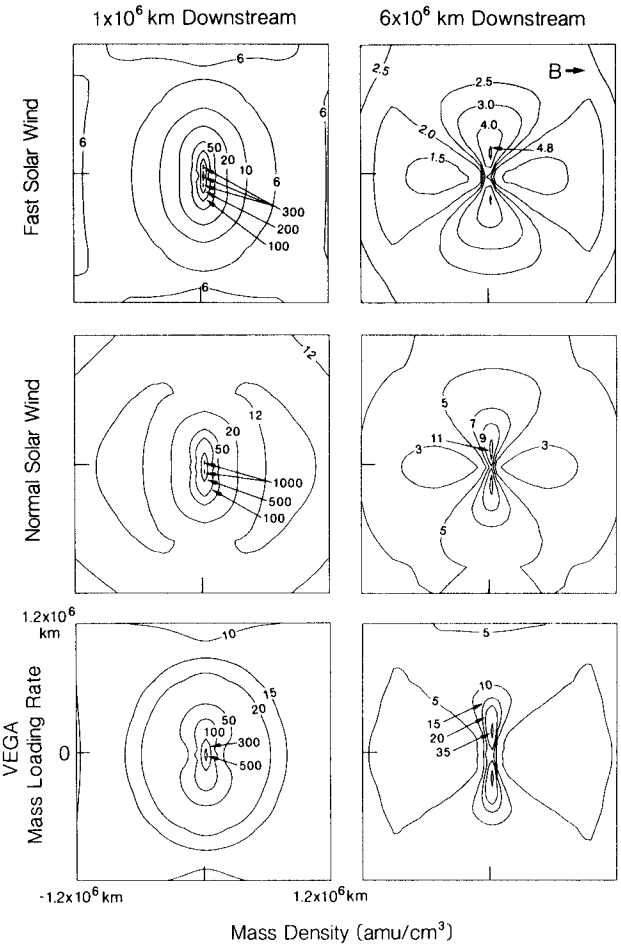

Fig. 6. Contour maps in planes perpendicular to the solar wind flow of total mass density at distances of 1 million and 6 million km downstream for the nucleus for the fast solar wind simulation (top), the normal solar wind simulation (middle) and the simulation using the VEGA outgassing rate (bottom). The upstream magnetic field is horizontal in these diagrams.

solar wind case in the center two panels, we see that there are two magnetic lobes of enhanced field strength at both distances separated by a narrow ribbon of reduced field strength corresponding roughly to the ion density ribbon seen in Figure 6. The minimum field strength in the center of the ion tail falls with distance down the tail in the model. The model is limited in its ability to resolve the narrowest minima in field strength or maxima in density. Nevertheless, the qualitative trends should be correct.

The fast solar wind cases are shown in the top 2 panels. They are very similar to the normal solar wind cases except that the field is about 2 nT stronger at large distances from the tail axis. The higher mass loading rate in the bottom two panels also makes very little difference in the

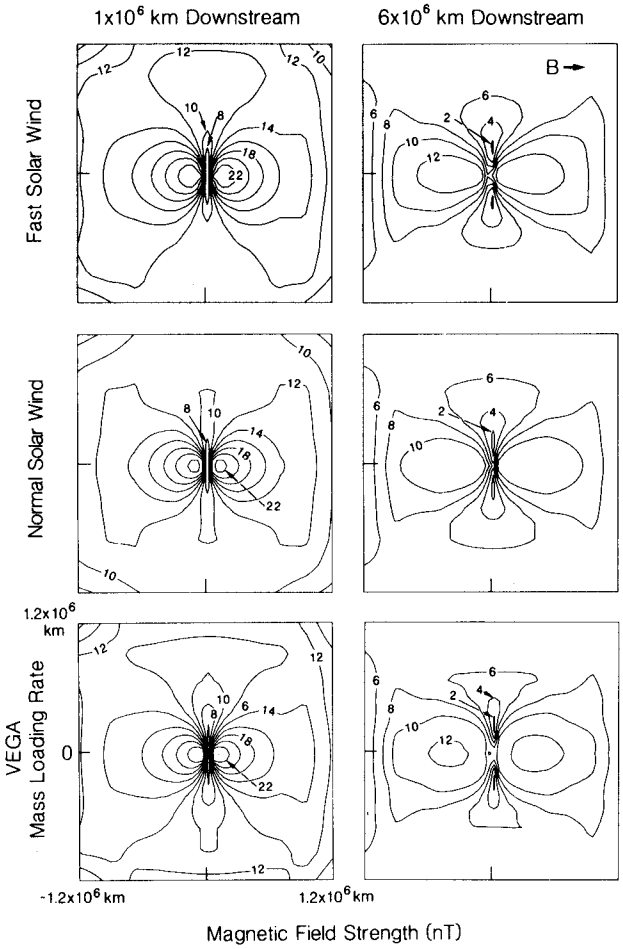

Fig. 7. Similar to Figure 6 but for the magnetic field strength.

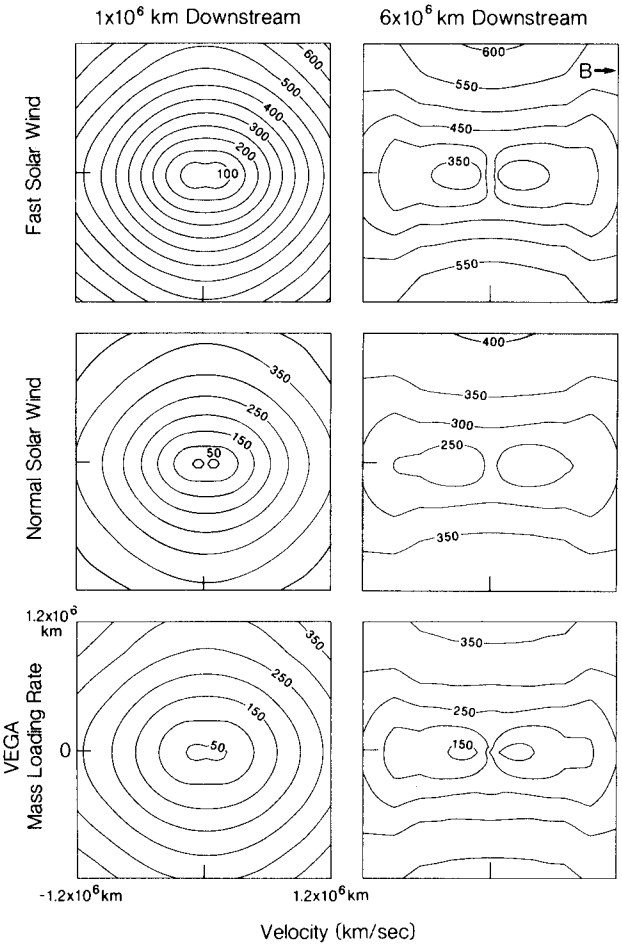

Fig. 8. Similar to Figure 6 but for the anti-solar component of the ion velocity.

field strength. At 10^6 km the field strength is about 2 nT greater but at 6 x 10^6 km it does not differ much from the normal solar wind case. As with the ion density contours the ribbons of field minima are slightly thinner, more ribbon-like and deeper. The lobes of maximum field strength are somewhat higher and larger in dimension.

Figure 8 shows contours of the anti-solar directed component of velocity for the three models. The behavior of all the models is similar. The anti-solar velocity is lowest near the nucleus and in the inner magnetic lobes. The velocity contours are stretched out along the magnetic field direction so that field lines that pass near the nucleus are moving more slowly over their entire length (at least over the interval contoured) than field lines that pass farther from the nucleus. The principal differences between these cases is that the fast solar wind case has the highest velocities and the high mass loading rate case has the lowest velocities. At 6 x 10^6 km the velocities in the high density ribbon is higher than that in the adjacent plasma. This is in accord with the acceleration of the ion tail in the anti-solar direction by the Lorentz force and the vanishing contribution of this force in the magnetic lobes. The field lines through the low velocity lobes cross the tail closer to the nucleus where the plasma in the ion tail is moving more slowly.

The solar wind interaction with a comet exerts a drag on the solar wind which decelerates it at the same time the cometary ions are accelerated. The region of solar wind deceleration is quite large compared to the visible ion tail. One way to study this acceleration and deceleration process is to examine the momentum flux moving down the tail. Figure 9 shows these contours in the same format as before. In the bottom 2 models the undisturbed momentum flux in the solar wind is 3.04 nPa and in the top 3.27 nPa. Thus at 1.0 million km downstream in the normal solar wind model the principal effect on the solar wind is a decrease in momentum flux over most of the region contoured with an enhancement in momentum flux in the ribbon of the ion tail. The transverse transfer of momentum flux

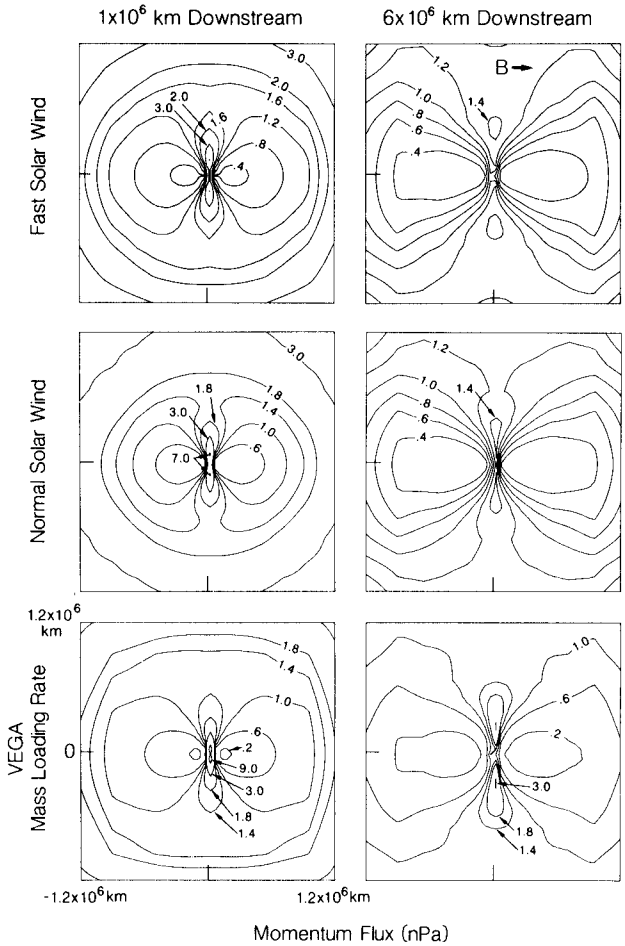

Fig. 9. Similar to Figure 6 but for the momentum flux.

from the neighboring solar wind streamlines to the tail proper is affected by the ability of the magnetic stresses to transport momentum along field lines. [cf. Schmidt and Wegmann, 1982]. At 6.0 million km the region of reduced momentum flux is larger and deeper and the momentum flux enhancement in the ion tail ribbon is reduced, presumably due to the spreading of the streamlines. There is very little difference here between the results for the fast and the normal solar winds. In the high mass loading rate model the region of reduced momentum flux is larger and the minima deeper. The momentum flux in the ion tail ribbon is similar to that of the normal solar wind at 1.0 million km and at 6.0 million km.

Discussion and Conclusions

Computer simulations provide an important adjunct to space observations even when the models do not duplicate the entire plethora of physical processes that are taking place because they allow the entire volume of the interaction to be probed and because they permit parametric studies to be undertaken. Our investigations with an MHD model [Fedder et al., 1986] have shown that magnetic draping and the pile-up of magnetic field lines varies as expected as the solar wind velocity varies and as the mass loading rate changes.

The visual appearance of a comet also depends on whether the magnetic field is in the plane of the sky or is orthogonal to it. When the comet is viewed along the interplanetary magnetic field direction the visible tail appears to be shorter. Hence rotations of the IMF should lead to apparent tail lengthenings and shortenings.

Finally, the comet both blocks the solar wind momentum flux over a wide area and accelerates the mass in the ion tail so that there is a region of reduced momentum flux surrounding a region of enhanced flux. It is possible that when the Earth passed through Halley's tail in 1910 such a region was indeed encountered [Russell et al., 1987, 1988].

Acknowledgments. The work at UCLA was supported by the National Aeronautics and Space Administration under grant NAGW-717.

References

Fedder, J. A., J. G. Lyon and J. L. Giuliani, Jr., Numerical simulations of comets: Predictions for comet Giacobini-Zinner, EOS, 67, 17-18, 1986.

Feldman, W. C., J. R. Asbridge, S. J. Bame and J. T. Gosling, Plasma and magnetic fields from the Sun, in The Solar Output and its Variation, ed. O. R. White, pp. 351-382, Colorado Assoc. Univ. Press, Boulder, Colorado, 1977.

Gringauz, K. I., et al., First in-situ plasma and neutral gas measurements at comet Halley, Nature, 321, 282, 1986.

Jockers, K., The ion tail of comet Kohoutek 1973 X11 during 17 days of solar wind gusts, Astron. Astrophys. Suppl. Ser., 62, 791-838, 1985.

Niedner, M. B., Jr. and J. Brandt, Interplanetary gas XX111. Plasma tail disconnection events in comets: Evidence for magnetic field reconnection at interplanetary sector boundaries, Astrophys. J., 223, 655, 1978.

Reinhard, R., The Giotto encounter with comet Halley, Nature, 321, 313, 1986.

Russell, C. T., M. A. Saunders, J. L. Phillips and J. A. Fedder, Near-tail reconnection as the cause of cometary tail disconnections, J. Geophys. Res., 91, 1417-1423, 1986.

Russell, C. T., J. L. Phillips, J. A. Fedder, J. H. Allen, L. Morris and R. A. Craig, Effect of possible passage through Halley's magnetic tail on geomagnetic activity, J. Geophys. Res., 92, 11195-11200, 1987.

Russell, C. T., M. von Dornum, R. L. McPherron, J. H. Allen and L. Morris, Geomagnetic activity during the passage of the Earth through Halley's tail in 1910, Nature, 333, 338-340, 1988.

Russell, C. T., G. Le, J. G. Luhmann and J. A. Fedder, The visual appearance of comets under varying solar wind conditions, Adv. Space Res., 9, (3)393-(3)396, 1989.

Schmidt, H. U. and R. Wegmann, MHD calculations for cometary plasmas, Comp. Phys. Com., 19, 309-326, 1980.

Schmidt, H. U. and R. Wegmann, Plasma flow and magnetic fields in comets, in Comets, edited by L. L. Wilkening, University of Arizona Press, Tucson, 1982.

Schwingenschuh, K., W. Riedler, G. Schelch, Ye. G. Yeroshenko, V. A. Styashkin, J. G. Luhmann, C. T. Russell and J. A. Fedder, Cometary boundaries: VEGA observations at Halley, Adv. Space Res., 6, 217, 1986.

Schwingenschuh, K., W. Riedler, Ye. G. Yeroshenko, J. L. Phillips, C. T. Russell, J. G. Luhmann and J. A. Fedder, Magnetic field draping in the comet Halley coma: Comparison of VEGA observations with computer simulations, Geophys. Res. Lett., 14, 640-643, 1987.